

Surface acoustic wave Fano interference in the quantum regime

J. M. Kitzman^{1,*}, J. R. Lane¹, C. Undershute¹, N. R. Beysengulov¹, C. A. Mikolas¹, K. W. Murch², and J. Pollanen^{1†}

¹*Department of Physics and Astronomy, Michigan State University, East Lansing, MI 48824, USA and*

²*Department of Physics, Washington University in St. Louis, St. Louis, MO 63130, USA*

Quantum acoustic systems, which integrate surface or bulk phonons with superconducting qubits, offer a unique opportunity to investigate phononic interference and scattering processes in the quantum regime. In particular the interaction between a superconducting qubit and a phononic oscillator allows the qubit to operate as a sensor of the oscillator’s excitation spectra and underlying interference effects. Here we present measurements revealing the interference of a resonantly trapped piezoelectric surface acoustic wave (SAW) mode and a broad continuum of surface phonons in a system consisting of a SAW resonator coupled to a superconducting qubit. By populating the SAW device with phonons we leverage the resulting ac Stark shift of the qubit to extract the mean excitation number of the surface phonon coherent state as a function of frequency. In this fashion, the qubit functions as a spectroscopic sensor of the surface phonon environment in the hybrid device and allows us to reveal the interaction between phonons in the resonant SAW mode and the broader surface phonon background, which is well-described within the context of Fano interference of surface piezo-phonons.

Wave interference is a universal phenomenon manifesting in a wide variety of both classical and quantum systems ranging from ocean waves to quantum circuits. The spectral response of these systems encodes the existence of the underlying interference processes, resonant modes, and their losses. A hallmark example is the Fano resonance [1–3], which arises from the interference between a resonantly scattered mode and a continuum of background states, and leads to a characteristically asymmetric spectral lineshape. Fano interference is a ubiquitous physical phenomenon and has been realized in numerous, fundamentally different, contexts in which sharp resonant modes interact with continuum excitations. This type of wave interference has been observed in atomic and molecular systems [4, 5], scattering in optical experiments [6, 7], and transport measurements in quantum dot-based condensed matter systems [8, 9]. The level of asymmetry in a Fano-lineshape is characterized by a parameter q , which depends on the phase shift across the continuum containing the resonant mode. When this phase shift is a sharply varying function of frequency, measurements of a Fano resonance offer a highly precise method for sensing [10–12]. Here we demonstrate the Fano-interference of resonantly trapped surface acoustic wave (SAW) phonons with a background of continuous phonon modes in an acoustic Fabry Pérot resonator that is cooled near its quantum mechanical ground state. We infer the surface phonon interference by measuring the absorption spectrum of a superconducting transmon qubit capacitively coupled to the SAW device, allowing the qubit to effectively operate as a sensor of the interfering SAW phonon environment.

Hybrid quantum systems utilizing the toolkit of circuit quantum electrodynamics (cQED) [13, 14] are an established and powerful platform for investigating the quantum mechanical properties of microwave photons. These systems have been used to reveal individual pho-

ton number states in an microwave field [15, 16], to create superpositions of microwave coherent states for generating logical qubits [17–19], and for creating highly interacting photonic bound states [20]. In an analogous fashion, circuit quantum acoustodynamics (cQAD) [21], in which the photonic degree of freedom is replaced with a phononic one, opens the door for investigating and controlling the quantum properties of vibrational excitations in solid state systems. In fact, experiments using the cQAD framework have shown the single phonon splitting of the absorption spectrum of a superconducting qubit [22–24], the generation of entangled states between spatially separated qubits mediated via phonons [25, 26], and the joint entanglement of high-frequency mechanical oscillators [27]. While a variety of phononic systems are available, architectures based on piezoelectric surface acoustic wave (SAW) devices allow for the tailoring of highly non-trivial surface phonon absorption spectra by leveraging the simulation machinery of the coupling of modes (COM) theory [28]. Using COM to design SAW-based hybrid systems experiments, it is now possible to create custom mechanical dissipation channels for investigating phononic open quantum systems [29], design multi-mode mechanical resonators that couple strongly to superconducting qubits [23, 30], and observe the negativity of acoustic Wigner functions [31].

Fig. 1a depicts a schematic of our experiment, which consists of a flux-tunable superconducting transmon qubit that interacts with a SAW device hosting a resonant mode at $\omega_m/(2\pi) = 4.4588$ GHz. The spectral response of the SAW device was precisely designed using the coupling-of-modes theory to define the electromechanical scattering properties of the device [28, 32], as shown in Fig. 1b. The effective electrical conductance of the SAW device was designed such that the resonantly confined acoustic mode is in close spectral proximity to a continuum of acoustic states (see Fig. 1b). To probe the

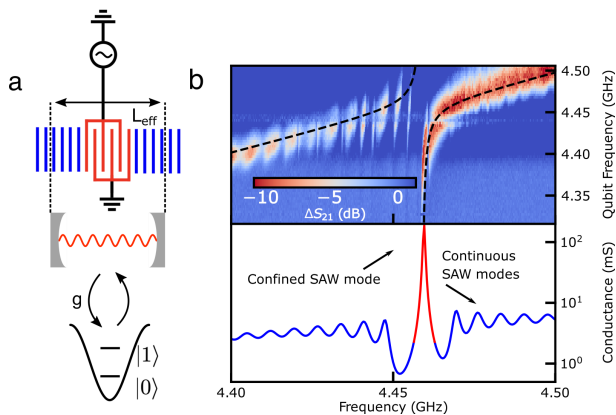


FIG. 1. (a) Schematic of the experiment. The phononic Bragg mirrors form a spatially distributed Fabry P erot cavity that allows for a coherent exchange of energy between the qubit and a resonantly confined SAW mode. (b) Top panel: Measurement of two-tone qubit spectroscopy as qubit is tuned through the main acoustic resonance and nearby SAW continuum. Strong coupling is seen between the confined acoustic mode while weaker coupling is seen between the qubit and the background of acoustic states. Bottom panel: Simulated mode structure for the SAW device, in which the confined acoustic mode is housed within a continuum of SAW states.

interaction between these various surface phonon modes we capacitively couple the SAW device to a flux tunable transmon qubit. The two devices are fabricated on separate substrates, with the SAW device on YZ-cut LiNbO₃ and the qubit on high-resistivity silicon. Both devices are galvanically connected to large antenna pads having an area 250 $\mu\text{m} \times 250 \mu\text{m}$ that form a pair of parallel plate capacitors between the two devices when they are assembled in a flip-chip configuration [33]. The capacitive coupling in this hybrid system ensures that strain in the piezoelectric SAW substrate induces a voltage across the qubit antennae, allowing for the exchange of energy between the qubit and SAW phonons (see Fig. 1a). The composite qubit-SAW system is housed in a 3D electromagnetic cavity with fundamental frequency $\omega_c/(2\pi) = 4.788$ GHz, which is used for qubit control and readout as well as for applying independent excitation tones to populate the SAW device. A superconducting coil wound around the cavity provides magnetic flux tunability of the resonant frequency of the qubit. As the resonant frequency of the qubit is tuned through the confined acoustic mode, we observe an avoided crossing of magnitude $g_m/(2\pi) = 9.76 \pm 0.60$ MHz (see Fig. 1b). Additional interactions between the qubit and phonon modes are also observed. In particular these features correspond to interactions between the qubit and phonons that are not strongly confined to the SAW resonator and therefore couple much more weakly to the qubit, manifesting as a series of dark states in the qubit spectra.

To utilize the qubit as a sensor of the surface phonon environment, we first calibrate the qubit response to

SAW excitations in the acoustic dispersive limit using the confined SAW resonance. In this regime the qubit frequency and spectral shape depend in an established and systematic fashion on the excitation number of SAW bosons. This ac Stark shift has been observed in superconducting qubit systems coupled to both microwave resonators in the cQED framework [16, 34] as well as mechanical oscillators of multiple cQAD architectures [21–24]. In this dispersive limit, the detuning between the qubit frequency (ω_q) and the resonant SAW mode (ω_m) is large compared to g_m ($g_m \ll |\Delta|$, $\Delta = \omega_q - \omega_m$). In particular we tune the qubit frequency such that $\Delta/(2\pi) = -138.6$ MHz, where we may approximate the

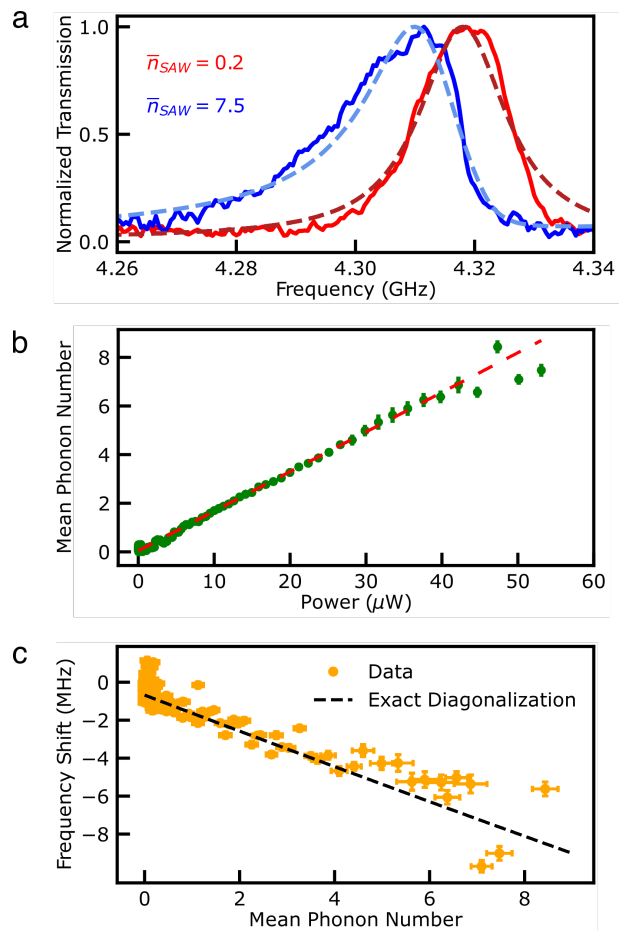


FIG. 2. (a) Representative qubit spectra at two different applied powers near resonance with the confined SAW mode. With increasing power the qubit spectrum both shifts in frequency and inherits a spectral lineshape expected from the statistics of the acoustic coherent state. (b) Measurement of mean phonon number as a function of drive power. The extracted phonon number follows the expected linear trend (red). (c) Qubit frequency shift versus extracted mean phonon number. Exact diagonalization considers the qubit as a 5 level atom, which agrees with the experiment.

Hamiltonian describing the hybrid system as ($\hbar = 1$) [13]

$$\hat{H} \simeq \omega_m (\hat{a}^\dagger \hat{a} + 1/2) + \frac{1}{2} \left(\omega_q + 2\chi_m \hat{a}^\dagger \hat{a} + \frac{g_m^2}{\Delta} \right) \hat{\sigma}_z. \quad (1)$$

In Eqn. 1 the SAW degrees of freedom are described by bosonic operators \hat{a} and \hat{a}^\dagger , and the qubit is described by the spin 1/2 operator $\hat{\sigma}_z$. The acoustic dispersive shift $2\chi_m = 2g_m^2/\Delta$ represents the shift of the effective qubit frequency with increasing SAW phonon number. Based on the experimental parameters of our system the qubit frequency shift per phonon at this detuning is $\chi_m/\pi = -1.372$ MHz. By applying a tone that is resonant with the confined acoustic mode we generate a coherent SAW state and subsequent measurement of the resulting qubit spectra allows us to measure the mean surface phonon number.

We fit the qubit spectra (see Fig. 2a) to an established model [15] consisting of a two level system coupled to a harmonic oscillator coherent state. The asymmetry of the qubit spectra at large excitation numbers (see Fig. 2a) arises from the quantum fluctuations in the phonon number in the resulting SAW coherent state. As shown in Fig. 2b we find a linear relationship between the drive power populating the SAW resonator and the extracted mean phonon number. Exact diagonalization of a multi-level Jaynes-Cummings Hamiltonian describing this coupled system allows us to extract the expected qubit frequency shift as a function of phonon number in the dispersive limit [30] and we find excellent agreement between this prediction and the measured phonon number as shown in Fig. 2c.

Having calibrated the frequency response of the qubit to phonons in the confined SAW resonance, we extend these Stark shift measurements to probe the acoustic environment outside of the stop-band of the SAW mirrors. We measure the acoustic Stark shift $\delta\omega_q$ as a function of drive frequency ω_d , and extract the mean phonon occupation $\bar{n} = |\delta\omega_q|/2\chi_m$ over a range of drive frequencies. As shown in Fig. 3a, the measured phonon number has a maximum at the resonant frequency of the confined acoustic mode $\omega_m/(2\pi) = 4.4588$ GHz, and is strikingly asymmetric about this peak. By design, the acoustic excitation spectrum hosts a rich structure near this confined resonance, making it possible for phonons across a range of frequencies to interfere with each other. Because the reflectivity of the mirrors that define the SAW cavity is relatively low ($\sim 0.5\%$ per mirror structure), the reflection process for surface phonons is distributed over the length of the cavity. This creates a situation in which phononic excitations that reflect at different spatial positions within the cavity interfere with each other either constructively or destructively depending upon their relative wavevectors and propagation paths. These interference processes produce to a Fano resonance, as phonons in the confined acoustic mode are subject to differing interference with surface phonons outside of the mirror

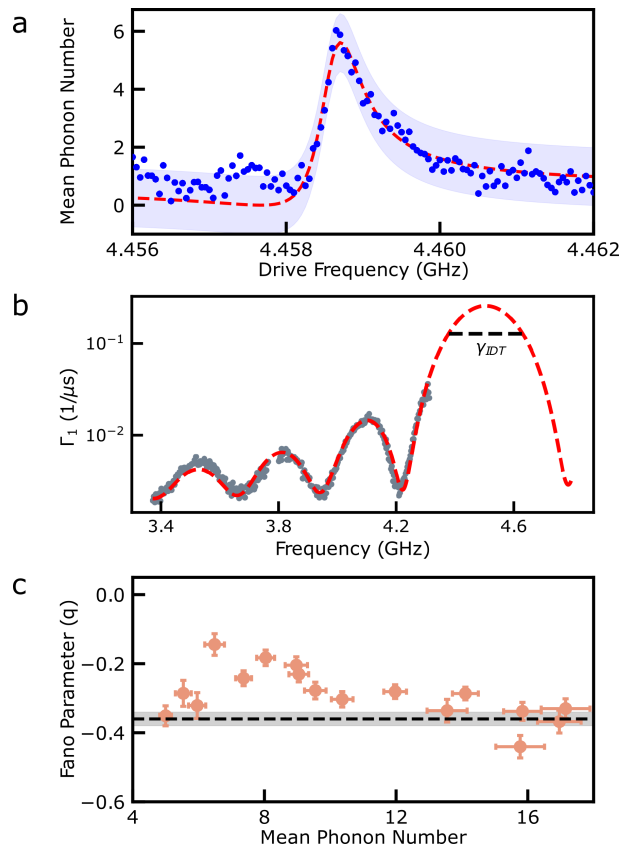


FIG. 3. (a) Mean phonon number as a function of SAW drive frequency at a fixed power of $P_{\text{drive}} = 25 \mu\text{W}$. The SAW resonance is asymmetric in frequency and is well-described by a Fano absorption function. The asymmetry arises from phonons in the confined acoustic mode interacting with phonons in the SAW continuum. The light blue band corresponds to a single phonon deviation from the fit (red) and represents a 95% confidence interval. (b) Measurement of the qubit decay rate over a broad range of frequencies far from the confined acoustic resonance. The fit (red) is to the analytical expression of the SAW-induced loss due to the central SAW transducer. The decay rate of the transducer is $\gamma_{\text{IDT}}/(2\pi) = 249.7$ MHz. (c) Fano asymmetry parameter q as a function of drive power. The black dashed line indicates q based on the analysis of two coupled harmonic oscillators.

stop-band depending on their frequency. We model the resulting frequency-dependent phonon number as a Fano resonance [2, 3] with an absorption spectra, $\bar{n}(\omega)$:

$$\bar{n}(\omega) = \bar{n}_{\text{max}} \left(1 + q^2 - \frac{(q\Gamma/2 + \omega - \omega_m)^2}{(\Gamma/2)^2 + (\omega - \omega_m)^2} \right). \quad (2)$$

Eqn. 2 depends on the linewidth, Γ , of the resonantly confined mode, as well as the Fano parameter q , which describes the level of interference between confined and lossy surface phonons. The first two terms in Eqn. 2 do not depend on frequency and impose the physical constraint that the minimum SAW phonon number is non-negative. We note that the limit $q \rightarrow 0$ corresponds to the absence of phonon interference, and in this limit a

Lorentzian response is recovered.

To determine the characteristic level of phonon interference in our device, we use the qubit to measure the phonon occupation near the confined acoustic mode as a function of the power used to populate the SAW device with phonons. By fitting each resulting phonon spectra using Eqn. 2 we determine the Fano parameter as a function of the maximum mean phonon number. These results provide a relative measure of the acoustic interference in the device and are displayed in Fig. 3c. In particular we find that the phonon interactions are well-described by Eqn. 2, with a negative Fano parameter, down to the lowest phonon levels we are able to measure. Additionally, we find that the phonon interference is roughly constant with $q \approx -0.3$ as a function of mean phonon number. We attribute the larger spread in q at low phonon number to the relative imprecision in fitting noisier phonon spectra arising from smaller phonon Stark shifts. Finally, we note that at higher phonon number, the qubit spectra become significantly broad and the maximum phonon number, estimated from fitting, inherits larger uncertainty, as indicated by the horizontal error bars in Fig. 3c.

To understand the level of interference we observe in our measurements, we compare the SAW phononic system to a minimal classical model of Fano interference arising in two coupled oscillators in which one oscillator has a significantly larger loss rate than the other [35]. In this model, the interaction between the two oscillators leads to Fano interference and allows us to calculate the parameter q . The loss rate of the confined acoustic mode, which corresponds to the low loss oscillator is measured as the linewidth extracted from the fit to the resonantly trapped SAW mode in Fig. 3a. The linewidth indicates that the loss of the confined mode is $\gamma_{\text{SAW}}/(2\pi) = 650 \pm 35$ kHz, corresponding to a SAW quality factor $Q_{\text{SAW}} \simeq 6500$. To estimate the loss rate of the significantly more lossy interdigitated transducer (IDT) response, we measure the qubit decay rate, $\Gamma_1 = 1/T_1$, as a function of qubit frequency far from the confined acoustic resonance. In this regime, the qubit loss is proportional to the electrical conductance [29, 36] of the SAW device, which is well described by only the IDT response far from the confined mode, where the mirror reflectivity is much less than one. In particular we fit Γ_1 to a phenomenological form taking into account loss resulting in the transduction of qubit excitations into phonons that exit the SAW mirrors,

$$\Gamma_1(\omega_q) = \frac{\omega_q}{2\pi Q_i} + \Gamma_0 \text{sinc}^2\left(\pi N_p \frac{\omega_q - \omega_{\text{IDT}}}{\omega_{\text{IDT}}}\right), \quad (3)$$

where $Q_i = 1.67 \times 10^3$ is the qubit internal quality factor, $\Gamma_0 = 0.252 \text{ ns}^{-1}$ is the maximum conversion rate of the qubit excitation into SAW phonons, $N_p = 16$ is the number of finger pairs in the IDT structure of the SAW resonator, and $\omega_{\text{IDT}}/(2\pi) = 4.504 \text{ GHz}$ is the cen-

tral transducer frequency, which is within 1% of the value predicted from the device fabrication parameters. By fitting the qubit loss to the response given by Eqn. 3 (see Fig. 3b), we are able to extract the overall loss associated with the central transducer, which we approximate as a Lorentzian with a width of $\gamma_{\text{IDT}}/(2\pi) = 249.7 \text{ MHz}$. In the limit where the response of the transducers is broad in frequency compared to that of the confined mode, as is the case in our experiments ($\gamma_{\text{SAW}}/\gamma_{\text{IDT}} \approx 0.3\%$), the Fano parameter can be calculated as [35],

$$q = \frac{1}{\gamma_{\text{IDT}} \omega_{\text{SAW}}} (\omega_{\text{SAW}}^2 - \omega_{\text{IDT}}^2). \quad (4)$$

Based on experimental parameters we calculate $q = -0.36 \pm 0.02$, which is indicated by the black dashed line and shaded region in Fig. 3b. As the maximum phonon number in the SAW device is varied, we observe excellent agreement between the measured Fano parameter and that predicted from Eqn. 4. In conclusion, we have demonstrated the Fano interference of surface acoustic wave phonons in a SAW device containing a single resonantly confined mode embedded in a continuum of SAW modes. This phononic interference is inferred from qubit-assisted spectroscopy of the SAW device and we find that it persists down to extremely low excitation number. The experimental results are in excellent qualitative agreement with the functional form of a Fano resonance and quantitatively agree with a minimal classical model of the Fano effect. These results also demonstrate the ability to engineer SAW-based quantum acoustic systems and leverage the sensitivity of superconducting qubits to a local piezo-phononic environment.

We thank M.I. Dykman, V. Zelevinsky, A. Schleusner, D. Kowsari, P.M. Harrington, and P.K. Rath for valuable discussions. We also thank R. Loloee and B. Bi for technical assistance and use of the W. M. Keck Microfabrication Facility at MSU. The Michigan State portion of this work was supported by the National Science Foundation (NSF) via grant number ECCS-2142846 (CAREER) and the Cowen Family Endowment at MSU. The Washington University portion of this work was also supported by the NSF via grant number PHY-1752844 (CAREER).

* kitzmanj@msu.edu

† pollanen@msu.edu

- [1] E. Majorana, *Nuovo Cimento* **8**, 22 (1931).
- [2] U. Fano, *Phys. Rev.* **124**, 1866 (1961).
- [3] A. E. Miroshnichenko, S. Flach, and Y. S. Kivshar, *Rev. Mod. Phys.* **82**, 2257 (2010).
- [4] C. Ott, A. Kaldun, P. Raith, K. Meyer, M. Laux, J. Evers, C. H. Keitel, C. H. Greene, and T. Pfeifer, *Science* **340**, 716 (2013), .
- [5] Y.-N. Lv, A.-W. Liu, Y. Tan, C.-L. Hu, T.-P. Hua, X.-B. Zou, Y. R. Sun, C.-L. Zou, G.-C. Guo, and S.-M. Hu,

- Phys. Rev. Lett. **129**, 163201 (2022).
- [6] M. I. Tribelsky, S. Flach, A. E. Miroschnichenko, A. V. Gorbach, and Y. S. Kivshar, Phys. Rev. Lett. **100**, 043903 (2008).
- [7] W. Zhao and Y. Jiang, Opt. Lett. **40**, 93 (2015).
- [8] K. Kobayashi, H. Aikawa, A. Sano, S. Katsumoto, and Y. Iye, Phys. Rev. B **70**, 035319 (2004).
- [9] A. C. Johnson, C. M. Marcus, M. P. Hanson, and A. C. Gossard, Phys. Rev. Lett. **93**, 106803 (2004).
- [10] B. Luk'yanchuk, N. I. Zheludev, S. A. Maier, N. J. Halas, P. Nordlander, H. Giessen, and C. T. Chong, Nature Materials **9**, 707 (2010).
- [11] S. Zhang, K. Bao, N. J. Halas, H. Xu, and P. Nordlander, Nano Letters **11**, 1657 (2011).
- [12] S. Xiao, Y. Yoon, Y.-H. Lee, J. P. Bird, Y. Ochiai, N. Aoki, J. L. Reno, and J. Fransson, Phys. Rev. B **93**, 165435 (2016).
- [13] A. Blais, R.-S. Huang, A. Wallraff, S. M. Girvin, and R. J. Schoelkopf, Phys. Rev. A **69**, 062320 (2004).
- [14] A. Blais, A. L. Grimsmo, S. M. Girvin, and A. Wallraff, Rev. Mod. Phys. **93**, 025005 (2021).
- [15] J. Gambetta, A. Blais, D. I. Schuster, A. Wallraff, L. Frunzio, J. Majer, M. H. Devoret, S. M. Girvin, and R. J. Schoelkopf, Phys. Rev. A **74**, 042318 (2006).
- [16] D. I. Schuster, A. A. Houck, J. A. Schreier, A. Wallraff, J. M. Gambetta, A. Blais, L. Frunzio, J. Majer, B. Johnson, M. H. Devoret, S. M. Girvin, and R. J. Schoelkopf, Nature **445**, 515 EP (2007).
- [17] B. Vlastakis, G. Kirchmair, Z. Leghtas, S. E. Nigg, L. Frunzio, S. M. Girvin, M. Mirrahimi, M. H. Devoret, and R. J. Schoelkopf, Science **342**, 607 (2013), .
- [18] N. Ofek, A. Petrenko, R. Heeres, P. Reinhold, Z. Leghtas, B. Vlastakis, Y. Liu, L. Frunzio, S. M. Girvin, L. Jiang, M. Mirrahimi, M. H. Devoret, and R. J. Schoelkopf, Nature **536**, 441 (2016).
- [19] J. M. Gertler, B. Baker, J. Li, S. Shirol, J. Koch, and C. Wang, Nature **590**, 243 (2021).
- [20] A. Morvan, T. I. Andersen, X. Mi, C. Neill, A. Petukhov, K. Kechedzhi, D. A. Abanin, A. Michailidis, R. Acharya, F. Arute, K. Arya, A. Asfaw, J. Atalaya, J. C. Bardin, J. Basso, A. Bengtsson, G. Bortoli, A. Bourassa, J. Bovaird, L. Brill, M. Broughton, B. B. Buckley, D. A. Buell, T. Burger, B. Burkett, N. Bushnell, Z. Chen, B. Chiaro, R. Collins, P. Conner, W. Courtney, A. L. Crook, B. Curtin, D. M. Debroy, A. Del Toro Barba, S. Demura, A. Dunsworth, D. Eppens, C. Erickson, L. Faoro, E. Farhi, R. Fatemi, L. Flores Burgos, E. Forati, A. G. Fowler, B. Foxen, W. Giang, C. Gidney, D. Gilboa, M. Giustina, A. Grajales Dau, J. A. Gross, S. Habegger, M. C. Hamilton, M. P. Harrigan, S. D. Harrington, M. Hoffmann, S. Hong, T. Huang, A. Huff, W. J. Huggins, S. V. Isakov, J. Iveland, E. Jeffrey, Z. Jiang, C. Jones, P. Juhas, D. Kafri, T. Khattar, M. Khezri, M. Kieferová, S. Kim, A. Y. Kitaev, P. V. Klimov, A. R. Klots, A. N. Korotkov, F. Kostritsa, J. M. Kreikebaum, D. Landhuis, P. Laptev, K.-M. Lau, L. Laws, J. Lee, K. W. Lee, B. J. Lester, A. T. Lill, W. Liu, A. Locharla, F. Malone, O. Martin, J. R. McClean, M. McEwen, B. Meurer Costa, K. C. Miao, M. Mohseni, S. Montazeri, E. Mount, W. Mroczkiewicz, O. Naaman, M. Neeley, A. Nersisyan, M. Newman, A. Nguyen, M. Nguyen, M. Y. Niu, T. E. O'Brien, R. Olenewa, A. Opremcak, R. Potter, C. Quintana, N. C. Rubin, N. Saei, D. Sank, K. Sankaragomathi, K. J. Satzinger, H. F. Schurkus, C. Schuster, M. J. Shearn, A. Shorter, V. Shvarts, J. Skrzuzny, W. C. Smith, D. Strain, G. Sterling, Y. Su, M. Szalay, A. Torres, G. Vidal, B. Villalonga, C. Vollgraf-Heidweiller, T. White, C. Xing, Z. Yao, P. Yeh, J. Yoo, A. Zalcman, Y. Zhang, N. Zhu, H. Neven, D. Bacon, J. Hilton, E. Lucero, R. Babbush, S. Boixo, A. Megrant, J. Kelly, Y. Chen, V. Smelyanskiy, I. Aleiner, L. B. Ioffe, and P. Roushan, Nature **612**, 240 (2022).
- [21] R. Manenti, A. Kockum, A. Patterson, T. Behrle, J. Rahamim, G. Tancredi, F. Nori, and P. Leek, Nature Communications **8**, 1 (2017).
- [22] P. Arrangoiz-Arriola, E. A. Wollack, Z. Wang, M. Pechal, W. Jiang, T. P. McKenna, J. D. Witmer, R. Van Laer, and A. H. Safavi-Naeini, Nature **571**, 537 (2019).
- [23] L. R. Sletten, B. A. Moores, J. J. Viennot, and K. W. Lehnert, Phys. Rev. X **9**, 021056 (2019).
- [24] U. von Lüpke, Y. Yang, M. Bild, L. Michaud, M. Fadel, and Y. Chu, Nature Physics (2022), 10.1038/s41567-022-01591-2.
- [25] A. Bienfait, K. J. Satzinger, Y. P. Zhong, H.-S. Chang, M.-H. Chou, C. R. Conner, É. Dumur, J. Grebel, G. A. Pears, R. G. Povey, and A. N. Cleland, Science **364**, 368 (2019), .
- [26] É. Dumur, K. J. Satzinger, G. A. Pears, M.-H. Chou, A. Bienfait, H.-S. Chang, C. R. Conner, J. Grebel, R. G. Povey, Y. P. Zhong, and A. N. Cleland, npj Quantum Information **7**, 173 (2021).
- [27] E. A. Wollack, A. Y. Cleland, R. G. Gruenke, Z. Wang, P. Arrangoiz-Arriola, and A. H. Safavi-Naeini, Nature **604**, 463 (2022).
- [28] D. P. Morgan, *Surface Acoustic Wave Devices*, 2nd ed. (Elsevier Ltd., 2005).
- [29] J. M. Kitzman, J. R. Lane, C. Undershute, P. M. Harrington, N. R. Beysengulov, C. A. Mikolas, K. W. Murch, and J. Pollanen, "Phononic bath engineering of a superconducting qubit," (2022).
- [30] B. Moores, L. Sletten, J. Viennot, and K. Lehnert, Phys. Rev. Lett. **120**, 227701 (2018).
- [31] K. J. Satzinger, Y. P. Zhong, H.-S. Chang, G. A. Pears, A. Bienfait, M.-H. Chou, A. Y. Cleland, C. R. Conner, É. Dumur, J. Grebel, I. Gutierrez, B. H. November, R. G. Povey, S. J. Whiteley, D. D. Awschalom, D. I. Schuster, and A. N. Cleland, Nature **563**, 661 (2018).
- [32] J. R. Lane, *Integrating Superconducting Qubits with Quantum Fluids and Surface Acoustic Wave Devices*, Ph.D. thesis, Michigan State University (2021).
- [33] A complete description of the assembled device can be found in Ref. [29].
- [34] D. I. Schuster, A. Wallraff, A. Blais, L. Frunzio, R.-S. Huang, J. Majer, S. M. Girvin, and R. J. Schoelkopf, Phys. Rev. Lett. **94**, 123602 (2005).
- [35] M. Iizawa, S. Kosugi, F. Koike, and Y. Azuma, Physica Scripta **96**, 055401 (2021).
- [36] A. A. Houck, J. A. Schreier, B. R. Johnson, J. M. Chow, J. Koch, J. M. Gambetta, D. I. Schuster, L. Frunzio, M. H. Devoret, S. M. Girvin, and R. J. Schoelkopf, Phys. Rev. Lett. **101**, 080502 (2008).